

A Robotic Bipedal Model for Human Walking with Slips

Kuo Chen, Mitja Trkov, Jingang Yi, Yizhai Zhang, Tao Liu, and Dezhen Song

Abstract—Slip is the major cause of falls in human locomotion. We present a new bipedal modeling approach to capture and predict human walking locomotion with slips. Compared with the existing bipedal models, the proposed slip walking model includes the human foot rolling effects, the existence of the double-stance gait and active ankle joints. One of the major developments is the relaxation of the non-slip assumption that is used in the existing bipedal models. We conduct extensive experiments to optimize the model parameters and to validate the proposed walking model with slips. The experimental results demonstrate that the model successfully predicts the human walking and recovery gaits with slips.

I. INTRODUCTION

The fall-related economic and societal costs for elders and professional workers are enormous. In the US only, the fall-related costs for the elderly were over \$19 billion dollars in 2000 and the costs are likely to increase in the future due to the aging population [1]. The fall-related injuries for professional workers also increase by 42% from 2008 to 2012 in the US [2]. Slip is one of the major causes for falling injuries. Modeling of walking locomotion with slips is critical for helping prevent these injuries and loss.

Slip-and-fall has been extensively studied in the past two decades, for example, [3], [4] and references therein. Most of these studies focus on human subjects and clinical experiments and few uses human locomotion dynamics to analyze the slipping mechanism. On the other hand, bipedal dynamics have been extensively used to design and control robotic walkers [5], predict the human walking gait and design the lower-limb prosthetic devices [6], [7]. However, all of these bipedal models assume non-slip conditions at the foot-floor contact and the results cannot be directly used to study locomotion with slips.

The goal of this study is to develop an analytic bipedal model for human walking with slips. We build a human bipedal model with actuated ankle joints. The model includes the dynamics of the both single- and double-stance motion.

The work was supported in part by the US NSF under award CMMI 1334389, National Natural Science Foundation of China under award 61428304 and the State Key Lab of Fluid Power Transmission and Control award GZKF-201404, Zhejiang University, China.

K. Chen, M. Trkov and J. Yi are with the Department of Mechanical and Aerospace Engineering, Rutgers University, Piscataway, NJ 08854 USA (email: kc625@rutgers.edu; mitja.trkov@rutgers.edu; jgyi@rutgers.edu).

Y. Zhang is with the Department of Control and Information, Northwestern Polytechnical University, Xi'an, Shaanxi 710072 China (e-mail: yzhang@nwpu.edu.cn).

T. Liu is with the Department of Mechanical Engineering, Zhejiang University, Hangzhou, Zhejiang 310027, China (email: liutao@zju.edu.cn).

D. Song is with the Department of Computer Science and Engineering, Texas A&M University, College Station, TX 77843 USA (e-mail: dzsong@cse.tamu.edu).

The model explicitly considers the foot contact slips and therefore, it can predict the human gait under slips. We conduct extensive human experiments to validate the model.

The main contributions of this work are twofold. First, for the first time this paper extends the robotic bipedal models to study human walking under foot slips. The new model not only predicts the human gait with slips, but also is helpful for understanding of the motion stability when slips happen. Second, besides relaxing the assumption of non-slip foot-floor contact, the new model brings innovative features and properties compared with the other existing bipedal models. For example, compared with the bipedal models with a point, a flat or multi-contact foot in [5], [8], the new model includes an experimentally validated foot contact shape. Unlike the bipedal model in [7] that only deals with single-stance human locomotion, the proposed model includes the human trunk and also the double-stance phase in walking gaits, which is crucial for slips and fall motion. Compared with the work in [6] that include the double-stance, the proposed model includes the active ankle joints and also generates the experiments-matched ground reaction forces (GRF) [9].

The rest of the paper is organized as follows. We first review the related work in Section II. In Section III, we present the bipedal dynamic model slips. The experiments are presented in Section IV. We conclude the paper in Section V.

II. RELATED WORK

The proposed slips-and-fall bipedal modeling work are related to several research topics such as slip biomechanics, bipedal robotics, and in-situ sensing of human motion.

Extensive research have been reported in studying biomechanics of foot slips and falls. To quantify the slipperiness and predict the slips, required coefficient of friction (RCOF), defined as a ratio of the total friction and normal forces between the shoe and the ground, is proposed and used [3]. To predict the real-time RCOF, the work in [10] use the kinematic relationship of the human body's center of mass (COM) and the center of pressure (COP) of the shoe-floor contact. In [4], a 7-link, 9-degree-of-freedom (DOF) walking model with a 16-element foot model is used to simulate the human reaction control to a novel slip in gait. In [11], a simulation model is optimized with human experiments and, stability results are obtained and compared with the dynamic balance analyses by a simple invented pendulum model. The 2D musculoskeletal model is also used in [12] to determine the impact of the reduced RCOF on gait kinematics.

Bipedal modeling and control are extensively in robotic walking design; see [5] and the references therein. Due to the foot impact on the ground in each strike, a hybrid dynamic

model is commonly used to describe the continuous dynamics in the single- or double-stance periods with discrete-switch mappings to capture the foot contact impacts. Point or flat foot models are employed in these bipedal robotic dynamics. Using the hybrid zero dynamics concept [13], a low-dimensional normal human walking model has been presented in [6] and a state feedback control is designed to track the gait profile parameterized by the stance phase variable, rather than time [5].

Use of the bipedal robotic dynamic models to study human locomotion is reported recently. In [6], the bipedal model is used to study human gaits with fixed ankle joints. Both the single- and double-stance phases are included in the model and a hybrid zero dynamic control is designed to track the human gait profile. Although the kinematic variables such as hip, knee and HAT (head, arms and trunk) joint angles match the human gaits, the predicted GRFs have large discrepancies with experiments. In [7], an optimization process is used to determine the values of the model parameters to match the human gaits. Only single-stance locomotion is considered in the model without the HAT. The kinematics of the model predictions match the human gaits and no predicted GRF results are reported. The models in [6], [7] use the circular curved foot-floor contact. All of the above-mentioned bipedal models are built on the assumption of no slips.

The measurement of slipperiness and the devices to measure the friction between the shoe and the floor are discussed in [14]. Force plate is the most commonly used device to measure the GRF and to calculate the foot contact COP. However, force plates cannot be used for monitoring daily activities outside the laboratory. In recent years, wearable insole pressure measurement devices were developed to obtain the normal GRF (e.g., [15]). We use an integrated sensor suite inside shoes to measure the 3D GRF. The details of these sensors are discussed in [9]. Combining with the wearable motion sensors (e.g., [16]), we obtain the limb poses and forces in indoor or outdoor environment.

III. BIPEDAL WALKING MODEL WITH SLIPS

A. System Configuration

Fig. 1(a) illustrates the setup of the coordinates for bipedal model. The human motion is considered only in the sagittal plane. The human body is considered as a 7-link rigid body. The HAT is considered as one link that is connected to the left- and right-thigh. The human has two active hip joints, two active knee joints and two active ankle joints. Similar to [7], we use relative angles q_i , $i = 2, \dots, 7$ to define the system configuration and absolute angle q_1 denotes the leading leg orientation with respect to the vertical direction.

We define $\mathbf{q}_a = [q_1 \ \dots \ q_7]^T$ as the gait configuration. The foot-floor contact is considered as a circular disk with radius R rolling on the solid ground; see Fig. 1(b). To capture the slip motion of stance foot, we denote the position of rotating center O_r of the stance foot rolling as $[x_o \ y_o]^T$. We define a slipping vector $\mathbf{q}_s = [x_s \ y_s]^T = [x_o + R\phi \ y_o - R]^T$, where ϕ is the absolute angle of the stance foot with respect to the vertical direction. It is straightforward to see that when

the stance foot is purely rolling on the ground, $\mathbf{q}_s = \mathbf{0}$. To completely determine the walking gait with slips, we define generalized coordinates $\mathbf{q}_e = [\mathbf{q}_a^T \ \mathbf{q}_s^T]^T$.

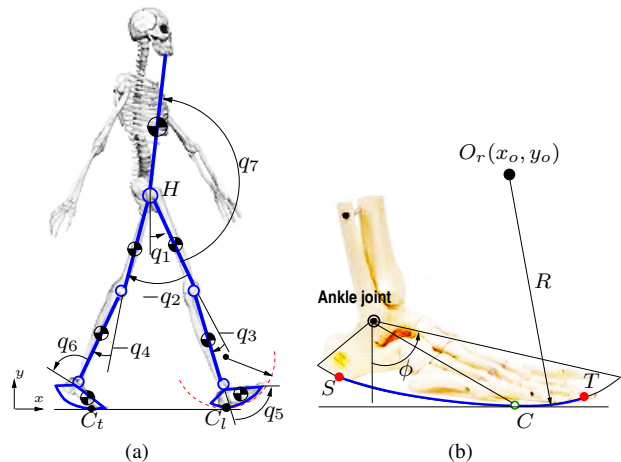


Fig. 1. (a) Schematic of the 7-link human walking model with curved foot contact. (b) Schematic of the foot-contact model.

A human walking cycle consists of a series of repeated sequential movements. The hybrid bipedal dynamics include the *single-stance phase* and the *double-stance phase* [5]. The hybrid model diagram shown in Fig. 2 captures the basic characteristics of the discrete-continuous dynamics.

B. Bipedal Dynamics without Slips

The non-slip single-stance dynamics are described as [5]

$$\Sigma_s : \mathbf{D}_s(\mathbf{q}_a)\ddot{\mathbf{q}}_a + \mathbf{C}_s(\mathbf{q}_a, \dot{\mathbf{q}}_a)\dot{\mathbf{q}}_a + \mathbf{G}_s(\mathbf{q}_a) = \mathbf{B}_s \mathbf{u}, \quad (1)$$

where $\mathbf{D}_s(\mathbf{q}_a)$, $\mathbf{C}_s(\mathbf{q}_a, \dot{\mathbf{q}}_a)$, $\mathbf{G}_s(\mathbf{q}_a)$ and \mathbf{B}_s are the inertia, Coriolis, gravity and input mapping matrices, respectively. There are six joint torque inputs $\mathbf{u} \in \mathbb{R}^6$ and the system is underactuation since absolute joint angle q_1 is not controlled by any joint torque. A feedback linearization approach is adopted to control the joint angles \mathbf{q}_a to follow a desired trajectory that is specified by a progression variable $\theta = \mathbf{c}\mathbf{q}_a$, where \mathbf{c} is a constant progression vector. The feedback linearization controller enforces the virtual constraint

$$\mathbf{y} = \mathbf{h}(\mathbf{q}_a) = \mathbf{H}_0 \mathbf{q}_a - \mathbf{h}_d(\theta) = \mathbf{0}. \quad (2)$$

The 7-link human walker is subject to gravitational force and stance foot GRF, including normal force F_n and tangential force F_x . During the double-stance phase, both the leading and trailing feet are in contact with the ground at contact points C_l and C_t , respectively, see Fig. 1(a). We here consider a general modeling approach by defining slipping vectors $\mathbf{g}_l(\mathbf{q}_e) \in \mathbb{R}^2$ and $\mathbf{g}_t(\mathbf{q}_e) \in \mathbb{R}^2$ of contact points C_l and C_t , respectively. Because of the constraints at the foot-floor contact, the equations of motion during the double-stance can be expressed as

$$\Sigma_d : \mathbf{D}_e(\mathbf{q}_e)\ddot{\mathbf{q}}_e + \mathbf{C}_e(\mathbf{q}_e, \dot{\mathbf{q}}_e)\dot{\mathbf{q}}_e + \mathbf{G}_e(\mathbf{q}_e) = \mathbf{B}_e \mathbf{u} + \mathbf{E}_e^T \mathbf{F}_e, \quad (3)$$

where $\mathbf{D}_e(\mathbf{q}_e)$, $\mathbf{C}_e(\mathbf{q}_e, \dot{\mathbf{q}}_e)$, $\mathbf{G}_e(\mathbf{q}_e)$ and \mathbf{B}_e are the inertia, Coriolis, gravity and input mapping matrices, respectively. Matrix $\mathbf{E}_e = [\frac{\partial \mathbf{g}_l(\mathbf{q}_e)}{\partial \mathbf{q}_e} \ \frac{\partial \mathbf{g}_t(\mathbf{q}_e)}{\partial \mathbf{q}_e}]^T \in \mathbb{R}^{4 \times 9}$ describes the

contact constraints and $\mathbf{F}_e = [F_{xt} \ F_{nt} \ F_{xl} \ F_{nl}]^T$ is a vector of the collection of the friction and normal forces at C_t and C_l . With non-slip conditions at C_l and C_t , we have four constraints $\mathbf{E}_e \dot{\mathbf{q}}_e = \mathbf{0}$ and the number of DOF of (3) is 5.

Because of six active joints and five degrees of freedom, the system is *overactuated*. Using a similar derivation in [6], the constrained dynamics can be reformulated as

$$\mathbf{D}_{di} \ddot{\mathbf{q}}_{di} + \mathbf{C}_{di} \dot{\mathbf{q}}_{di} + \mathbf{G}_{di} = \mathbf{M}_{di} \mathbf{u}, \quad (4)$$

where subscript ‘‘di’’ denotes double-stance independent variables, $\mathbf{q}_{di} = [q_1 \ q_2 \ q_3 \ q_5 \ q_7]^T$ and $\mathbf{M}_{di} \in \mathbb{R}^{5 \times 6}$ maps the six joint torques into the five dimensional dynamics. We take a simple linear constraint of the joint torques by the single-stance joint torque profiles to fully determine \mathbf{u} . To predict double-stance human gaits by (4), a Bézier polynomial is used to parameterize the desired trajectory of \mathbf{q}_{di}^d [5].

To calculate \mathbf{F}_e , we take time derivative of kinematic constraint $\mathbf{E}_e \dot{\mathbf{q}}_e = \mathbf{0}$. Stacking with (3), we obtain (argument variables in the coefficient matrices are dropped for clarity)

$$\begin{bmatrix} \mathbf{D}_e & -\mathbf{E}_e^T \\ \mathbf{E}_e & \mathbf{0} \end{bmatrix} \begin{bmatrix} \ddot{\mathbf{q}}_e \\ \mathbf{F}_e \end{bmatrix} = \begin{bmatrix} \mathbf{B}_e \\ \mathbf{0} \end{bmatrix} \mathbf{u} - \begin{bmatrix} \mathbf{C}_e \\ \dot{\mathbf{E}}_e \end{bmatrix} \dot{\mathbf{q}}_e - \begin{bmatrix} \mathbf{G}_e \\ \mathbf{0} \end{bmatrix}. \quad (5)$$

Since coefficient matrix is full rank, both $\ddot{\mathbf{q}}_e$ and forces \mathbf{F}_e are obtained with the known \mathbf{u} . We express the impact mapping \mathcal{H}_s^d as the pre-impact joint velocity $\dot{\mathbf{q}}_e^-$ of the single-stance phase to the post-impact joint velocity $\dot{\mathbf{q}}_e^+$ of the double-stance phase as

$$\mathcal{H}_s^d : \begin{bmatrix} \mathbf{D}_e(\mathbf{q}_e^-) & -\mathbf{E}_e^T \\ \mathbf{E}_e & \mathbf{0} \end{bmatrix} \begin{bmatrix} \dot{\mathbf{q}}_e^+ \\ \delta \mathbf{F}_e \end{bmatrix} = \begin{bmatrix} \mathbf{D}_e(\mathbf{q}_e^-) \dot{\mathbf{q}}_e^- \\ \mathbf{0} \end{bmatrix}. \quad (6)$$

Also, we know that $\mathbf{q}_e^+ = \mathbf{q}_e^-$. The transition from the double-stance to single-stance phases is obtained as $\mathcal{H}_d^s : \mathbf{q}_e^+ = \mathbf{q}_e^-$, $\dot{\mathbf{q}}_e^+ = \dot{\mathbf{q}}_e^-$.

To apply the bipedal model to human gait, we need to tune the model parameters to fit the human walking data. For single-stance dynamics (1), we need to identify and match the virtual constraint $\mathbf{h}(\mathbf{q}_a)$ in (2) from the collected joint angles. The desired trajectory \mathbf{h}_d is parameterized by the Bézier polynomial. To fit the double-stance model (3), we choose to optimize the Bézier spline parameters α_d such that the desired trajectory $\mathbf{q}_{di}^d = \mathbf{q}_{di}^d(\alpha_d, t)$ approximates the human walking. We take the joint angular acceleration into the optimization process because the GRF matching is one of the targets besides the joint angles. To achieve such goal and obtain optimal α_d , we minimize

$$J_d(\alpha_d) = \int_{t_0}^{t_f} \|\mathbf{q}_{di}^d(\alpha_d, t) - \mathbf{q}_{di}^e\|^2 + \gamma \|\ddot{\mathbf{q}}_{di}^d(\alpha_d, t)\|^2 dt,$$

where $\gamma > 0$ is a weighting factor and $[t_0, t_f]$ is the time interval and \mathbf{q}_{di}^e is the measured joint angle profiles. By the property of the Bézier polynomials, optimal α_d can be obtained using a scaled conjugate gradient method.

C. Bipedal Model with Slips

Fig. 2 shows the finite state diagram of the hybrid bipedal model with slips. For the normal walking gait, the hybrid

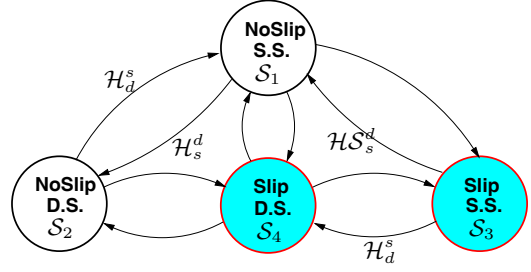


Fig. 2. Finite state diagram of human walking gait with slips.

dynamics contain two states: non-slip single-stance (\mathcal{S}_1) and double-stance (\mathcal{S}_2) phases.

The foot slip can happen during the single- and double-stance phases. Therefore, two new states are introduced for the gaits with slip: single-stance slip phase \mathcal{S}_3 and double-stance slip phase \mathcal{S}_4 . State \mathcal{S}_4 includes the cases where slip happens on the stance leg only, the swing leg only, or the both legs simultaneously. The transitions shown in the figure represent the human slip recovery strategies. For example, as we will show in the case study in Section IV, one slip recovery strategy can be represented in the sequence of $\mathcal{S}_1 \rightarrow \mathcal{S}_4 \rightarrow \mathcal{S}_3 \rightarrow \mathcal{S}_1$. The human starts with normal single-stance \mathcal{S}_1 without slip. Slip is initiated right after the swing leg touches on the ground (\mathcal{S}_4). When slip evolves, the swing leg is lifted off the ground so the walking gait is in single-stance slip phase (\mathcal{S}_3). Then, the swing leg touches down on the ground and becomes a non-slip stance leg. Meanwhile, the other slipping leg leaves the ground contact and the gait recovers to the non-slip single-stance phase (\mathcal{S}_1). The details of each transition in the finite state diagram are out of the scope of this paper.

Due to slips, we use $\mathbf{q}_e = [\mathbf{q}_a^T \ x_s \ y_s]^T$ to describe the motion. The dynamic model is obtained as

$$\begin{bmatrix} \mathbf{D}_{es}^{11} & \mathbf{D}_{es}^{12} \\ \dots & \dots \\ \mathbf{D}_{es}^{21} & \mathbf{D}_{es}^{22} \\ \dots & \dots \\ \mathbf{D}_{es}^{31} & \mathbf{D}_{es}^{32} \\ \dots & \dots \end{bmatrix} \begin{bmatrix} \ddot{\mathbf{q}}_a \\ \ddot{x}_s \\ \ddot{y}_s \end{bmatrix} + \begin{bmatrix} \mathbf{C}_{es}^{11} & \mathbf{C}_{es}^{12} \\ \dots & \dots \\ \mathbf{C}_{es}^{21} & \mathbf{C}_{es}^{22} \\ \dots & \dots \\ \mathbf{C}_{es}^{31} & \mathbf{C}_{es}^{32} \\ \dots & \dots \end{bmatrix} \begin{bmatrix} \dot{\mathbf{q}}_a \\ \dot{x}_s \\ \dot{y}_s \end{bmatrix} + \begin{bmatrix} \mathbf{G}_{es}^1 \\ \mathbf{G}_{es}^2 \\ \dots \\ \mathbf{G}_{es}^3 \\ \dots \end{bmatrix} = \begin{bmatrix} \mathbf{B}_{es} \mathbf{u} \\ \mathbf{F}_x \\ \dots \\ \mathbf{F}_n \end{bmatrix} = \begin{bmatrix} \mathbf{B}_{es} \mathbf{u} \\ \mathbf{F}_{es} \end{bmatrix}, \quad (7)$$

where $\mathbf{D}_{es} \in \mathbb{R}^{9 \times 9}$, $\mathbf{C}_{es} \in \mathbb{R}^{9 \times 9}$, $\mathbf{G}_{es} \in \mathbb{R}^9$ and $\mathbf{B}_{es} \in \mathbb{R}^{7 \times 6}$ are the inertia, Coriolis, gravity and input mapping matrices, respectively. External force $\mathbf{F}_{es} = [F_x \ F_n]^T$ is the friction and normal forces at the stance foot.

Note that the stance foot always lies in contact with the ground during slipping and therefore, we have constraint $y_s = 0$. Also, we have $F_x = -\mu F_n$, where μ is the friction coefficient between the shoe and the floor. With these constraints, we simplify (7) by defining $\mathbf{q}_{es} = [\mathbf{q}_a \ x_s]^T \in \mathbb{R}^8$ and eliminating F_n and finally obtain

$$\mathbf{M}_{es}^s : \mathbf{D}_{es}^s \ddot{\mathbf{q}}_{es} + \mathbf{C}_{es}^s \dot{\mathbf{q}}_{es} + \mathbf{G}_{es}^s = \mathbf{B}_{es}^s \mathbf{u}, \quad (8)$$

where

$$\mathbf{D}_{es}^s = \begin{bmatrix} \mathbf{D}_{es}^{11} \\ \mathbf{D}_{es}^{21} + \mu \mathbf{D}_{es}^{31} \end{bmatrix}, \mathbf{C}_{es}^s = \begin{bmatrix} \mathbf{C}_{es}^{11} \\ \mathbf{C}_{es}^{21} + \mu \mathbf{C}_{es}^{31} \end{bmatrix} \in \mathbb{R}^{8 \times 8},$$

$$\mathbf{G}_{es}^s = \begin{bmatrix} \mathbf{G}_{es}^1 \\ \mathbf{G}_{es}^2 + \mu \mathbf{G}_{es}^3 \end{bmatrix} \in \mathbb{R}^8, \mathbf{B}_{es}^s = \begin{bmatrix} \mathbf{B}_{es} \\ \mathbf{0} \end{bmatrix} \in \mathbb{R}^{8 \times 6}.$$

System (8) has eight state variables and six joint torques as inputs and therefore, it is underactuated. The absolute joint angle q_1 and the slipping distance x_s are underactuated variables. To use model (8) for human gait prediction, we adopt a similar controller for non-slip case. A six-dimensional holonomic virtual constraint $\mathbf{y} = \mathbf{h}(\mathbf{q}_a) = \mathbf{H}_0 \mathbf{q}_a - \mathbf{h}_d(\theta_s)$ is used, where $\theta_s = \mathbf{c}_s \mathbf{q}_a$ and \mathbf{c}_s is chosen to insure $[\mathbf{H}_0^T \mathbf{c}_s^T]^T$ has full rank. Similar to the non-slip case, the control \mathbf{u} is designed to drive the outputs (and their derivatives) to zero and the zero dynamics can be obtained. Indeed, the dynamics of \dot{x}_s are part of the zero dynamics of the system.

During the double-stance slip gait, either only one of two feet slips while the other foot purely rolls on the ground, or both feet slide on the ground. These two situations share the same equations of motion (3) but with different governing constraints. For the first case, we always define the non-slipping leg as the stance leg and from the stance leg, we define the absolute joint angle q_1 , see Fig. 1(a). For the second case, we take either leg as the stance leg.

By such arrangements, for the first case, without loss of generality, we assume that the trailing leg is non-slip, stance leg and have constraints $\mathbf{g}_t(\mathbf{q}_e) = \mathbf{0}$ and $(\mathbf{g}_t(\mathbf{q}_e))_2 = 0$, where $(\mathbf{g}_i(\mathbf{q}_e))_j$, $i = l, t$, $j = 1, 2$, represents the j th coordinate of slipping vector $\mathbf{g}_i(\mathbf{q}_e)$. Moreover, we have the kinetic constraints $F_{xl} = -\mu F_{nl}$ for slipping foot. Similarly, for the second case, we have kinematic constraints $(\mathbf{g}_t(\mathbf{q}_e))_2 = (\mathbf{g}_l(\mathbf{q}_e))_2 = 0$ and kinetic constraints $F_{xt} = -\mu F_{tn}$ and $F_{xl} = -\mu F_{nl}$. We here only present the first case and similar results can be obtained for the second case.

Because of constraints $\mathbf{g}_t(\mathbf{q}_e) = \mathbf{0}$ and $\mathbf{g}_l(\mathbf{q}_e)_2 = 0$, we obtain $\frac{\partial \mathbf{g}_t}{\partial \mathbf{q}_e} \dot{\mathbf{q}}_e = \mathbf{0}$ and $\frac{\partial (\mathbf{g}_l(\mathbf{q}_e))_2}{\partial \mathbf{q}_e} \dot{\mathbf{q}}_e = 0$. Using the definition of \mathbf{E}_e in (3), these kinematic constraints are written into $\mathbf{E}_{es} \dot{\mathbf{q}}_e = \mathbf{0}$, where $\mathbf{E}_{es} := (\mathbf{E}_e)_{[1,2,4]} \in \mathbb{R}^{3 \times 9}$ is a matrix formed by taking rows 1, 2 and 4 of \mathbf{E}_e . Similarly, the kinetic constraint is used to re-write the force vector in (3) as

$$\mathbf{F}_e = \underbrace{\begin{bmatrix} 1 & 0 & 0 \\ 0 & 1 & 0 \\ 0 & 0 & -\mu \\ 0 & 0 & 1 \end{bmatrix}}_{\mathbf{C}_f} \underbrace{\begin{bmatrix} F_{xt} \\ F_{nt} \\ F_{nl} \end{bmatrix}}_{\mathbf{F}_{e3}} = \mathbf{C}_f \mathbf{F}_{e3}. \quad (9)$$

By taking derivative of velocity constraint $\mathbf{E}_{es} \dot{\mathbf{q}}_e = \mathbf{0}$ and stacking with the simplified (3) and (9), we obtain

$$\underbrace{\begin{bmatrix} \mathbf{D}_e & -\mathbf{E}_e^T \mathbf{C}_f \\ \mathbf{E}_{es} & \mathbf{0} \end{bmatrix}}_{\mathbf{D}_{\text{ext}}^s} \begin{bmatrix} \dot{\mathbf{q}}_e \\ \mathbf{F}_{e3} \end{bmatrix} = \underbrace{\begin{bmatrix} \mathbf{B}_e \\ \mathbf{0} \end{bmatrix}}_{\mathbf{B}_{\text{ext}}^s} \mathbf{u} - \underbrace{\begin{bmatrix} \mathbf{C}_e \\ \dot{\mathbf{E}}_{es} \end{bmatrix}}_{\mathbf{C}_{\text{ext}}^s} \dot{\mathbf{q}}_e - \underbrace{\begin{bmatrix} \mathbf{G}_e \\ \mathbf{0} \end{bmatrix}}_{\mathbf{0}}.$$

Matrix $\mathbf{D}_{\text{ext}}^s$ has full rank and therefore $\dot{\mathbf{q}}_e$ and \mathbf{F}_{e3} are uniquely determined once the current state variables and joint torques \mathbf{u} are given. Since the three dimensional constraints

$\mathbf{E}_{es} \dot{\mathbf{q}}_e = \mathbf{0}$ are enforced, the degrees of freedom of the system are $9 - 3 = 6$. Therefore, the system is *fully actuated*.

Letting $\mathbf{q}_i = [q_1 \ q_2 \ q_3 \ q_4 \ q_5 \ q_7]^T = \mathbf{S} \mathbf{q}_e$ be the independent variables, where $\mathbf{S} \in \mathbb{R}^{6 \times 9}$ is a constant transformation matrix from \mathbf{q}_e to \mathbf{q}_i , we express $\ddot{\mathbf{q}}_i = \mathbf{S}(\mathbf{D}_{\text{ext}}^s)^{-1} \mathbf{B}_{\text{ext}}^s \mathbf{u} + \mathbf{D}_{\text{ext}}^s{}^{-1} \mathbf{C}_{\text{ext}}^s$, where $\mathbf{S} \mathbf{D}_{\text{ext}}^s{}^{-1} \mathbf{B}_{\text{ext}}^s \in \mathbb{R}^{6 \times 6}$ is a full rank matrix. To track a given trajectory \mathbf{q}_i^d , the controlled joint torque is designed through feedback linearization.

The impact model under slip can be obtained from the results for the non-slip case. The main difference is that the slip can happen right after the impact and therefore, the velocity of heel-touch contact point C_l is possibly nonzero, unlike zero in non-slip case. From the previous discussion, we have the velocity constraint $\mathbf{E}_e \dot{\mathbf{q}}_e = \mathbf{v}_{\text{slip}} = [0 \ 0 \ v_{\text{slip}} \ 0]^T$, where v_{slip} is the slipping velocity of C_l (along the x -axis direction) after the heel-touch impact. Therefore, we obtain

$$\mathcal{H}S_s^d : \begin{bmatrix} \mathbf{D}_e(\mathbf{q}_e^-) & -\mathbf{E}_e^T \\ \mathbf{E}_e & \mathbf{0} \end{bmatrix} \begin{bmatrix} \dot{\mathbf{q}}_e^+ \\ \delta \mathbf{F}_e \end{bmatrix} = \begin{bmatrix} \mathbf{D}_e(\mathbf{q}_e^-) \dot{\mathbf{q}}_e^- \\ \mathbf{v}_{\text{slip}} \end{bmatrix}. \quad (10)$$

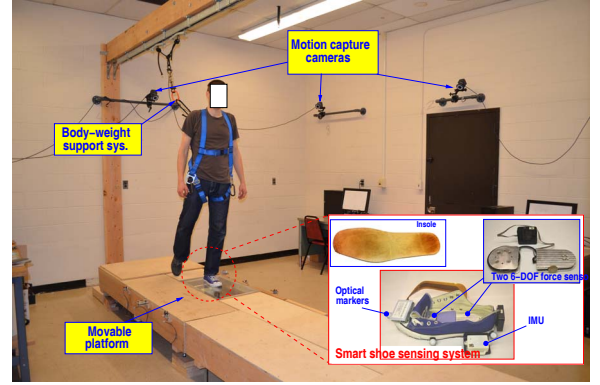


Fig. 3. The slip and fall experimental setup with various sensor suites.

IV. EXPERIMENTS

Fig. 3 shows the experimental setup for this study. The human subjects walk on the wooden platform in the laboratory. The human subject is first asked to walk on the platform to become familiar with the testing environment before he is asked to walk on the platform with reduced friction coefficients. The portion of the platform with the reduced coefficient of friction is not noticeable to the subject such that he keeps the normal gait before slip starts.

The human walking gait is captured by the optical motion tracking system (8 Bonita cameras from Vicon Inc.). Two six degree-of-freedom (6-DOF) force/torque sensors (model SS-1 from INSENCO Co., Ltd) are located inside the shoe to measure the 3D GRF and torques of the foot-floor contact; see Fig. 3. The GRF sensors and the motion capture system are synchronized for data collection. The details of discussion about the experimental setup are reported in [9].

We test and validate the foot rolling geometry using the normal walking motion data. Fig. 4(a) shows the foot center of pressure (COP) trajectory in the ankle frame. The data confirm the circular shape of the rolling model with radius $R = 0.22$ m. Fig. 4(b) further shows the comparison results

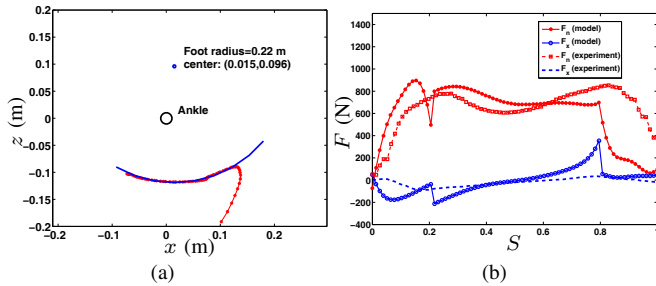


Fig. 4. (a) The foot-floor contact rolling geometry. The red stars indicate the COP trajectory in the ankle frame and the blue curve is the fitting circular shape. (b) GRF (F_n and F_x) of the stance leg without slips.

of the GRF (F_n and F_x) of the stance leg. Unlike the diverge results in literature (e.g., [6]), the model prediction results follow the trend of the force measurements. The discontinuity of the predicted GRF takes place at the phase switching moments due to the calculation errors of the joint angle accelerations from the models.

We next demonstrate the model prediction results for slip recovery gait experiment. Fig. 5(a) shows a snapshot of the slip recovery gait. The human starts the normal gait with a single-stance phase (\mathcal{S}_1 in Fig. 2) at $t = 0$ s. At $t = 0.32$ s, the (left) swing leg touches down on the slippery floor and then starts slipping. At this moment, the (right) foot is still in touch with the floor without slip and the human gait lies in double-stance slip phase (\mathcal{S}_4). At $t = 0.61$ s, the (right) swing foot leaves the ground (toe-off) and the (left) stance foot still slips. The gait enters the single-stance slip phase (\mathcal{S}_3). The walker quickly reacts the slip event. At $t = 0.96$ s the (right) swing foot touches down, the (left) stance foot leaves the ground and the gait becomes a recovered single-stance phase without slipping (\mathcal{S}_1). Fig. 5(b) shows the human skeleton data measured by the motion capture system and Fig. 5(c) demonstrates the skeleton constructed by the model predicted joint angles.

Fig. 6 shows the seven joint-angle comparison results of the model prediction and the measurements by the motion capture system. The results clearly confirm that the model prediction follows the experiments closely in the entire gait recovery process. Fig. 6(h) shows the slipping distance comparison and again, the model prediction follows the experiment. Figs. 7(a) and 7(b) show the normal and tangential GRF for the both feet. The GRF comparison clearly show that except the double-stance slip case during $t = 0.32$ to 0.61 s, the GRF predictions match the measurements. However, during the double-stance slip period, the force prediction are not accurate. We are currently working on improvement of these double-stance force calculations. Fig. 7(c) shows the coefficient of friction (COF) of the stance-foot contact during the slip recovery process. Before slips start (around 0.32 s), the required (actual) COF lies in a range of $|\mu| < 0.2$, which is far less than the available foot-floor friction coefficient (measured as close to 1 of the dry rubber-wood contact [9]). At $t = 0.32$ s, the available COF is less than 0.05 due to the fluidic soap film on surface. As shown in Fig. 7(c), the required COF is around $\mu = 0.05$,

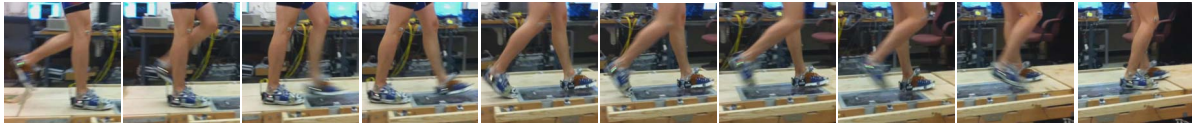
which is much smaller than the available COF. Therefore, slip starts when the foot touches down at that moment.

V. CONCLUSIONS

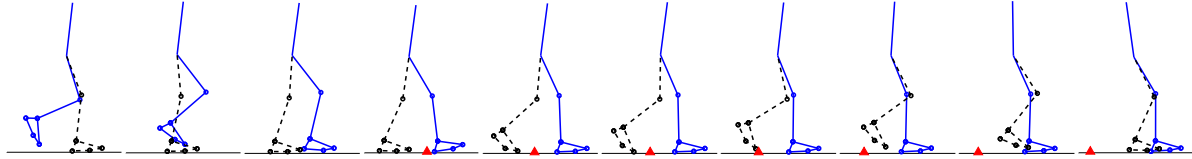
This paper presented a robotic bipedal dynamic model for human walking gait with foot slips. We relaxed the non-slip assumption used in the existing bipedal robotic models. A general hybrid bipedal model and the gait controllers were developed for human walking with foot slips. Experiments were conducted using the wearable force sensors to capture the ground reaction forces during the normal no-slip walking and the slipping recovery gaits. The comparison results confirmed that the model prediction match the experiments in both the joint angles and the GRF, which has not been reported previously. The new bipedal model can be potentially used for developing assistive robotic systems to prevent human from falling due to slips.

REFERENCES

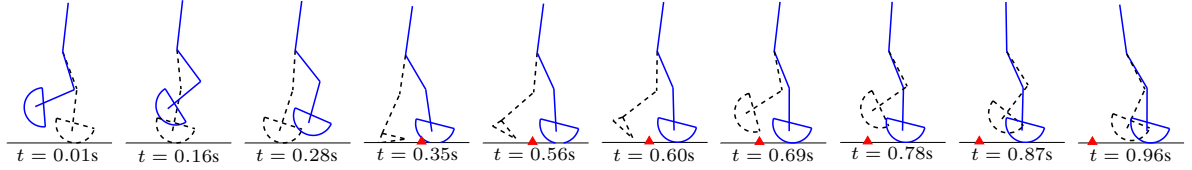
- [1] J. A. Stevens, P. S. Corso, E. A. Finkelstein, and T. R. Miller, "The costs of fatal and non-fatal falls among older adults," *Inj. Prev.*, vol. 12, pp. 290–295, 2006.
- [2] <http://www.libertymutualgroup.com>.
- [3] M. S. Redfern, R. Cham, K. Gielo-Perczak, R. Grönqvist, M. Hirvonen, H. Lanshammar, C. Y.-C. Pai, and C. Power, "Biomechanics of slips," *Ergonomics*, vol. 44, no. 13, pp. 1138–1166, 2001.
- [4] F. Yang and Y.-C. Pai, "Reactive control and its operation limits in responding to a novel slip in gait," *Ann. Biomed. Eng.*, vol. 38, no. 10, pp. 3246–3256, 2010.
- [5] E. R. Westervelt, J. W. Grizzle, C. Chevallereau, J. H. Choi, and B. Morris, *Feedback Control of Dynamic Bipedal Robot Locomotion*. Boca Raton, FL: CRC Press, 2007.
- [6] S. Srinivasan, "Low-dimensional modeling and analysis of human gait with application to the gait of transtibial prosthesis users," Ph.D. dissertation, Dept. Mech. Eng., Ohio State Univ., Columbus, OH, 2007.
- [7] A. E. Martin and J. P. Schmiedeler, "Predicting human walking gaits with a simple planar model," *J. Biomech.*, vol. 47, pp. 1416–1421, 2014.
- [8] D. J. Braun and M. Goldfarb, "A control approach for actuated dynamic walking in biped robots," *IEEE Trans. Robotics*, vol. 25, no. 6, pp. 1292–1303, 2009.
- [9] M. Trkov, J. Yi, T. Liu, and K. Li, "Shoe-floor interactions during human slip and fall: Modeling and experiments," in *Proc. ASME Dyn. Syst. Control Conf.*, San Antonio, TX, 2014, Paper DSCC2014-6184.
- [10] J. M. Burnfield and C. M. Power, "The role of center of mass kinematics in predicting peak utilized coefficient of friction during walking," *J. Forensic Sci.*, vol. 52, no. 6, pp. 1328–1333, 2007.
- [11] J. Patton, Y.-C. Pai, and W. A. Lee, "Evaluation of a model that determines the stability limits of dynamic balance," *Gait Posture*, vol. 9, pp. 38–49, 1999.
- [12] A. Mahboobin, R. Cham, and S. J. Piazza, "The impact of a systematic reduction in shoe-floor friction on heel contact walking kinematics - A gait simulation approach," *J. Biomech.*, vol. 43, pp. 1532–1539, 2010.
- [13] E. R. Westervelt, J. W. Grizzle, and D. E. Koditschek, "Hybrid zero dynamics of planar biped walkers," *IEEE Trans. Automat. Contr.*, vol. 48, no. 1, pp. 42–56, 2003.
- [14] R. Grönqvist, W.-R. Chang, T. K. Courtney, T. B. Leamon, M. S. Redfern, and L. Strandberg, "Measurement of slipperiness: Fundamental concept and definitions," *Ergonomics*, vol. 44, no. 13, pp. 1102–1117, 2001.
- [15] T. Liu, Y. Inoue, K. Shibata, and K. Shiojima, "A mobile force plate and three-dimensional motion analysis system for three-dimensional gait assessment," *IEEE Sensors J.*, vol. 12, no. 5, pp. 1461–1467, 2012.
- [16] Y. Zhang, K. Chen, J. Yi, and L. Liu, "Pose estimation in physical human-machine interactions with application to bicycle riding," in *Proc. IEEE/RSJ Int. Conf. Intell. Robot. Syst.*, Chicago, IL, 2014, pp. 3333–3338.



(a)



(b)



(c)

Fig. 5. A snapshot of the recovery human gait from slip. (a) Video snapshot. (b) Human 7-link skeleton from the optical motion capture system. The empty-circle dots indicate the reflective optical marker locations. (c) Skeleton prediction by the bipedal model. In (b) and (c), a red triangle is plotted to indicate the location where the left leg starts slipping.

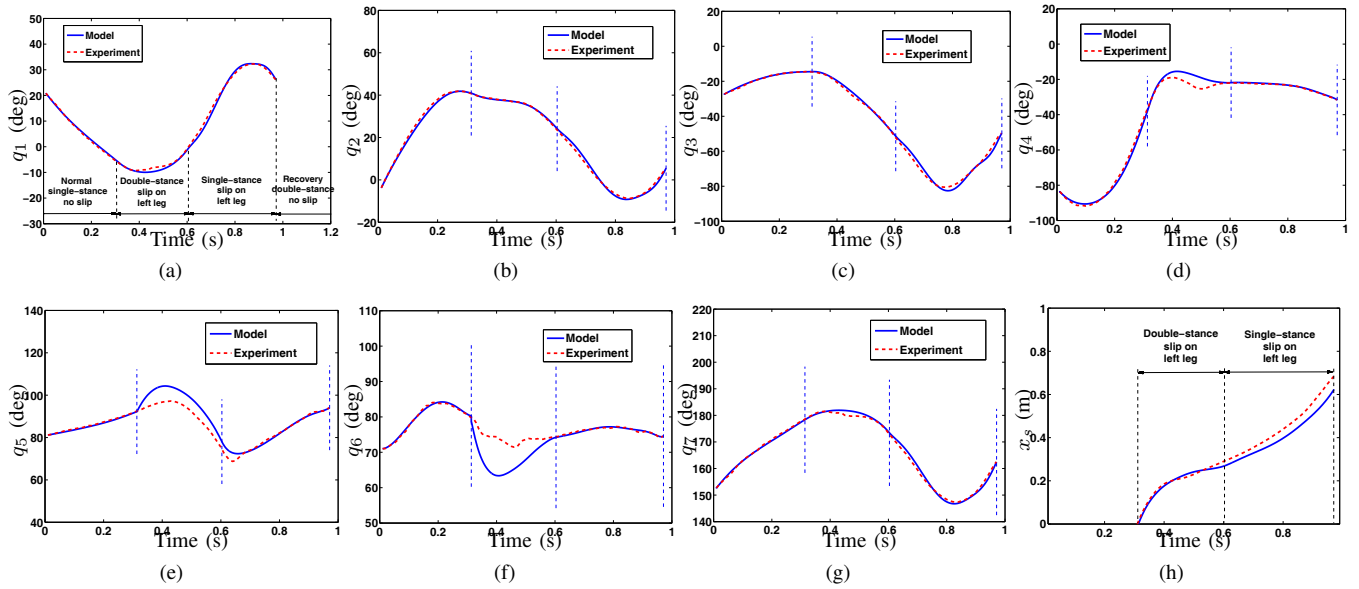


Fig. 6. (a)-(g): Joint angle (q_1 to q_7) comparisons between the model prediction and the experiments during slip recovery gait. The solid lines represent the model predictions and the dash lines show the experimental data. (h) Slipping distance x_s of the (left) stance leg during the slip recovery experiment.

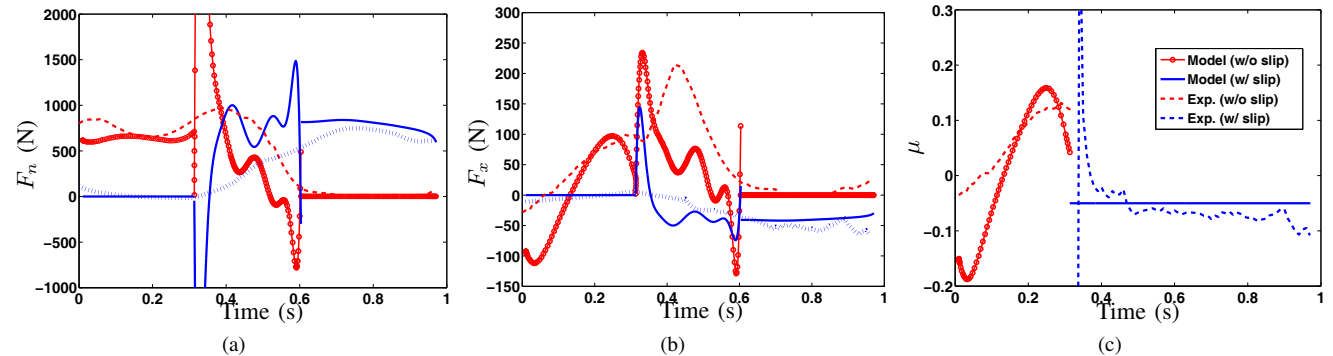


Fig. 7. Comparison results of the GRF and friction coefficient during the slip recovery. (a) Normal GRF F_n . (b) Tangential GRF F_x . (c) Friction coefficient μ of the stance leg foot. In (a) and (b), the model prediction forces for the left- and right legs are plotted as the blue solid and red circle lines, respectively, and the experiments are plotted as the blue dotted and the red dash lines. In (c), the model predicted and experimental μ in non-slip phase is plotted by the red empty circle and the dash lines, respectively, and these in the slip phase by the blue solid and dash lines, respectively.